Research Square

Preprints are preliminary reports that have not undergone peer review.
They should not be considered conclusive, used to inform clinical practice,
or referenced by the media as validated information.

Single-Time Selective Weight Redistribution in T-Symmetry-Broken BEC Bright Solitons via Itō Field Reversal: Density, Norm, and ABL Probability Diagnostics

Ikechukwu C. Okoro[1,2]

Ikechukwu.Okoro@nileuniversity.edu.ng

Delta State University https://orcid.org/0009-0008-3864-1758

Research Article

Keywords: T-symmetry breaking, Aharonov-Bergmann-Lebowitz (ABL) probability, Itō field reversal, Dynamical collapse asymmetry, BEC bright soliton

Posted Date: July 21st, 2026

DOI: https://doi.org/10.21203/rs.3.rs-10396152/v1

License: This work is licensed under a Creative Commons Attribution 4.0 International License.
Read Full License

Additional Declarations: The authors declare no competing interests.

Single-Time Selective Weight Redistribution in T-Symmetry-Broken BEC Bright Solitons via Itō Field Reversal: Density, Norm, and ABL Probability Diagnostics

Ikechukwu C. Okoro[1,2]*

[1]Department of Physics, Delta State University, Abraka, Nigeria

[2]Department of Physics, Nile University of Nigeria, Abuja, Nigeria

*Corresponding Author: Ikechukwu.Okoro@nileuniversity.edu.ng

Abstract

Testing quantum macroscopic irreversibility consistent with objective collapse constitute a major challenge of existing collapse models, because these models do not reconfigure the system's boundary conditions from first principles. This motivates our companion work which constructs asymmetry forward-backward noise-driven collapse via Itō reversal and martingale-type reduction in a stochastic CQ - NLSE. However, while the framework equations generally establishes T-symmetry breaking at the dynamical level and presents the generator, it is silent on the phenomenology of the collapse asymmetry. The present paper empirically probes further into the precise phenomenology by formulating three-diagnostic framework. In particular, we derive the particle density, norm, and the Aharonov-Bergmann-Lebowitz (ABL) formalism, to diagnose the T-symmetry breaking phenomenology in attractive ^{7}Li or ^{85}Rb bright-soliton condensates. Across all three diagnostics, the backward branch is consistently suppressed relative to the forward branch, which carries the larger weight. The norm is conserved and merely redistributed between the two branches: the joint ABL probability depends only on κ and is exactly invariant under ω, while the redistribution ratio between branches depends only on ω and is invariant under κ**.** The central finding, therefore, is that collapse asymmetry manifests as a redistribution of probability weights, rather than decaying as genuine decoherence phenomenology. We recommend a controllable BEC bright-soliton measurement of the ABL probability branches, targeting a null asymmetry gap ($|\Delta P^{ABL}| = 0$), would constitute a direct experimental test of this redistribution mechanism.

Keywords: T-symmetry breaking; Aharonov-Bergmann-Lebowitz (ABL) probability; Itō field reversal; Dynamical collapse asymmetry; BEC bright soliton.

1.0. INTRODUCTION

The major class of problems associated with quantum measurement incompatibility is how and why a single preferred outcome emerges upon measurement from a superposition of multiple possible quantum states before measurement [1, 2]. Dynamical collapse models have addressed this problem significantly by proposing nonlinear and stochastic modifications of standard quantum mechanics [3–6]. Several experimental probes of deviations predicted by collapse models from standard deterministic Schrödinger evolution have yielded promising results. Over a dozen active research groups are dedicated to collapse model experiments whose signatures can be sought via two broad experimental strategies, namely interferometric and non-interferometric tests [5–7]. While the former naturally detect the action of collapse by measuring corresponding interference signatures, the latter directly measure the stochastic diffusion activated by the collapse noise, which increases the system's translational and internal energies [8].

Among conventional approaches to testing collapse models, non-interferometric tests are gaining increasing attention because they have proved to be the most consistent across a wide range of systems. These systems include ultracold cantilevers [9, 10], gravitational wave detectors [11, 12], spontaneous X-ray emission [13–15], cold-atom anomalous heating [8], photon excitation [16], levitated optomechanical oscillators [17], and astrophysical observations [18]. Collectively, these experiments focus on probing specific parameter regions of the Continuous Spontaneous Localization (CSL) model — collapse rate λ and correlation length r_c. The goal is to eventually span the entire theoretically motivated CSL parameter space, resulting in either disproving CSL entirely or triggering a major adjustment of its parameters [19].

CSL collapse noise strength influences both the collapse rate and correlation length. The collapse noise must be sufficiently strong to suppress macroscopic superpositions — requiring a large collapse rate — yet sufficiently weak to preserve microscopic quantum coherence, requiring a large correlation length r_c and small collapse rate. The implication of these two conditions is that the theoretically feasible domain for the CSL collapse rate is narrow, $\lambda_{GRW} \sim 10^{-16}\,s^{-1}$ as proposed by Ghirardi, Rimini and Weber [3]. Constraining the experimentally excluded parameter regions must proceed from both large and small collapse rates, but the exclusion bounds advance asymmetrically. This asymmetry remains a major obstacle for non-interferometric tests [7, 10, 15,16, 19].

Soliton dynamics via Feshbach resonance mimic CSL collapse dynamical phenomena [20]. These include self-focusing instability [21], bosenova implosion and remnant release [20], and Itō field reversal asymmetry [22], analogous to CSL spatial asymmetry, collapse events, and T-symmetry breaking [6], respectively. These dynamics uniquely occur in BEC bright soliton propagation, governed by the stochastic CQ-NLSE with Itō noise [4, 22], making BEC bright solitons a genuine physical platform for the simulation and experimental probing of CSL-analogous collapse phenomena. This builds directly on the companion analysis [23], which derived the forward-to-backward amplitude ratio and growth-rate structure at the equation-of-motion level for the same stochastic Itō field-reversed CQ-NLSE pair.

Independent of any specific collapse model, time symmetry in quantum mechanics is itself a long-standing and currently active area of foundational research. The Aharonov-Bergmann-Lebowitz (ABL) formalism [28] assigns probabilities to intermediate measurement outcomes conditioned symmetrically on both an earlier (pre-selected) and a later (post-selected) boundary state, rather than privileging the initial condition alone as in standard quantum mechanics; this time-symmetric structure was later generalized into the broader two-state-vector formalism. Because the ABL construction treats past and future boundary conditions on an equal footing by design, any asymmetry it reveals when applied to a specific dynamics cannot be attributed to the measurement scheme itself, making it a natural, model-independent diagnostic of genuine time-reversal symmetry breaking. This question remains far from settled: Ridley [33] showed that quantum probabilities, including the ABL rule itself, can be derived from the temporal structure of a multiple-time wavefunction defined on the Keldysh contour, while Ridley and Adlam [34] more recently demonstrated that several existing time-symmetric interpretations of quantum mechanics fail to respect a stricter notion of event symmetry, proposing a fixed-point formulation that restores it across sequences of measurement events.

Independently, norm and particle density are standard signatures of T-symmetry breaking in nonlinear wave systems. For instance, T-reversal symmetry dictates reciprocity; violating it means forward and backward dynamics are no longer equal, and this non-reciprocity is directly associated with the norm of the wave [35]. In the dissipative CSL model [36], localization is introduced directly in terms of particle-number density rather than individual-particle coordinates, avoiding the difficulties of T-symmetric extension for identical particles. Both in the nonlinear-wave and

dynamical-collapse formulations, whether the resulting asymmetry survives as a genuine two-time, pre- and post-selected probability structure, or reduces to a trivial artifact of norm and density redistribution, has not been tested in the literature.

This paper formulates a diagnostic framework for collapse asymmetry and T-symmetry breaking via three complementary observables — particle density, norm, and ABL probability — derived from the same stochastic equations of motion. Together, these provide a genuine signature of the actual phenomenology of the asymmetry and T-symmetry breaking.

The remaining sections of this paper are organized as follows. Section 2 presents the analytical derivation of the three diagnostics, with the ABL probabilities from the carrier wave momentum eigenstate on the stochastic path toward the collapse threshold. Section 3 presents the results and discussion of T-symmetry breaking and collapse asymmetry signatures. Section 4 provides the summary.

2.0. THEORETICAL FORMULATION

2.1. Stochastic Nonlinear Directional Solitonic Equations

We are interested in the nonlinear dynamics of BEC bright solitons in which time-reversal asymmetry and collapse are studied. This is captured by the truncated stochastic framework, which integrates Itō field reversal and time-reversal asymmetry. The asymmetry arises quantitatively in the quintic collapse-coupling between the forward and backward dynamics, perturbed by a stochastic noise field. This results in the cubic-quintic nonlinear Schrodinger equation (CQ-NLSE) given as [22]:

$$i\frac{\partial \Phi_f}{\partial t} = -\frac{\partial^2 \Phi_f}{\partial x^2} + U_0|\Phi_f|^2\Phi_f - \frac{\omega}{8}|\Phi_f|^4\Phi_f\,, \tag{1a}$$

$$i\frac{\partial \Phi_b}{\partial t} = -\frac{\partial^2 \Phi_b}{\partial x^2} + U_0|\Phi_b|^2\Phi_b - \frac{5\omega}{8}|\Phi_b|^4\Phi_b\,, \tag{1b}$$

where $\Phi_f(\Phi_b)$ represent forward (backward) evolving order parameter, $U_0<0$ is attractive interaction, $\omega>0$ is driving frequency. The quintic nonlinearity coefficients, $\frac{\omega}{8}$ and $\frac{5\omega}{8}$, play dual role: (i) They stabilize the energy scale at which collapse dynamics is feasible, connecting the stochastic field to the quantum-optical frequency ω of the condensate mode, (ii) They provide

amplitude saturation for forward and backward propagations. Physically, ω and 5ω represent the strength of the attractive quintic interaction, which for a real condensate would require tuning via Feshbach resonance; the explicit mapping between this coupling and the Feshbach-tuned scattering length is not derived here and is left for future work.

The solutions of Equations (1a) and (1b) can take the form of variational ansatz of bright soliton, whose amplitudes are determined by the stability condition $2\omega<\kappa^2$ of the CQ-NLSE energy functional [24], rather than exact PDEs propagation. The bright solitons ansatz of forward and backward Equations (1a)-1(b) in the comoving frame $u=0$ can admit the form:

$$\Phi_f=\sqrt{\frac{4}{\omega}\left(1+\sqrt{1+\omega^2}\right)}\,\mathrm{sech}(\kappa x)e^{-i(\kappa x-\omega t)},$$

(2a)

$$\Phi_b=\sqrt{\frac{4}{5\omega}\left(1+\sqrt{1+5\omega^2}\right)}\,\mathrm{sech}(\kappa x)e^{-i(\kappa x+\omega t)},$$

(2b)

where κ is the wave-number, u is stationary velocity, x is coordinate position in 1D.

2.2. Forward and Backward Particle Densities

The particle density is defined as $\rho(x,t)=|\Phi|^2$ and using Equations (2a) and (2b) respectively:

$$\rho_f=\frac{4\left(1+\sqrt{1+\omega^2}\right)}{\omega}\mathrm{sech}^2\left(\kappa(x-ut)\right)$$

(3a)

$$\rho_b=\frac{4\left(1+\sqrt{1+5\omega^2}\right)}{5\omega}\mathrm{sech}^2\left(\kappa(x+ut)\right)$$

(3b)

2.3. Forward and Backward Norms

The soliton norm measures the total particle number in the system. This essentially controls probability conservation and reversibility of the evolution.

The norm is defined as :

$$N=\int_{-\infty}^{+\infty}\rho(x,0)dx$$

(4)

From Equation (3.34), the initial density is $\rho(x,0)=A^2\mathrm{sech}^2\kappa x$. As a result,

$$N = \int_{-\infty}^{+\infty} A^2 \operatorname{sech}^2 \kappa x dx$$

(5)

Using the standard integral $\int_{-\infty}^{+\infty} \operatorname{sech}^2 kx dx = \frac{2}{\kappa}$ and Equation (5) give the norms:

$$N_f = \frac{8\left(1+\sqrt{(1+\omega^2)}\right)}{\kappa\,\omega},$$

(6a)

$$N_b = \frac{8\left(1+\sqrt{(1+5\,\omega^2)}\right)}{5\kappa\,\omega}.$$

(6b)

In the strong-confinement limit in which the harmonic trap potential dominates completely over the cubic-quintic nonlinear self-interaction, we have the ratio:

$$\lim_{\omega\to\infty} \frac{N_f}{N_b} = \sqrt{5}.$$

(7)

It is worth nothing from Equations (6a) and (6b) that the vanishing derivatives $\frac{dN}{dt} = 0$ show that the norms are conserved in both branches.

2.4. Forward - Backward ABL Probabilities and Joint Probability

To establish the T-symmetry breaking diagnostics, the Aharonov-Bergmann-Lebowitz (ABL) probability [23, 25, 28] assigns a time-symmetric transition probability to a quantum measurement outcome α_m. This outcome α_m is conditioned on both pre-selected/ forward soliton $|\Phi_f\rangle$ and the post-selected / backward soliton $|\Phi_b\rangle$, evolving from either boundary condition under the directional CQ-NLSE (1a)-(1b). We define the joint ABL probability distribution:

$$P_{f/b}^{ABL} = \frac{|\langle\Phi_b|\alpha_m\rangle|^2 |\langle\alpha_m|\Phi_f\rangle|^2}{|\langle\Phi_b|\Phi_f\rangle|^2},$$

(8)

and the asymmetry gap:

$$\left|\Delta P^{ABL}\right| = \left|P_f^{ABL} - P_b^{ABL}\right|,$$

(9)

where the forward and backward ABL probabilities are respectively,

$$P_f^{ABL} = |\langle\alpha_m|\Phi_f\rangle|^2$$

(10a)

$$P_b^{ABL} = |\langle \Phi_b | \alpha_m \rangle|^2$$

(10b)

Equation (8) is bilinear in the forward and backward solitons, and physically encodes the macroscopic quantum interference between the forward and backward conditions mediated by $|\alpha_m\rangle$.To evaluate the ABL probabilities, we choose the momentum-space projection in κ, conveyed in the plane-wave phase factor of the solitons $e^{\pm i(\kappa x)}$:

$$\alpha_m = \frac{1}{\sqrt{2\pi}} e^{i(\kappa x)}$$

(11)

This is physically consistent since the momentum is naturally conserved in the large frequency limit $\omega \to \infty$ [26], moreover the measurement of momentum is standard experimental observable in cold-atom BEC settings, using time-of-flight technique [27]. The solitons remain in comoving frame achieved by a Galilean transform $x \to x - ut$, eliminating the x-dependent drift in the soliton phase without changing the collapse dynamics.

From Equation (10a), the co-ordinate space representation is the integral:

$$\langle \alpha_m | \Phi_f \rangle = \int_{-\infty}^{+\infty} \alpha_m^*(x)\, \Phi_f(x,t) dx,$$

(12)

using the standard integral $\int_{-\infty}^{+\infty} \mathrm{sech}(kx) dx = \frac{\pi}{k}$;

$$\langle \alpha_m | \Phi_f \rangle = \frac{e^{-i\omega t}}{\kappa} \sqrt{\frac{2\pi}{\omega}\left(1+\sqrt{1+\omega^2}\right)}.$$

(13)

Taking the modulus squared:

$$P_f^{ABL} = |\langle \alpha_m | \Phi_f \rangle|^2 = \frac{2\pi}{\omega\kappa^2}\left(1+\sqrt{1+\omega^2}\right).$$

(14)

Defining the integral of Equation (10b):$\langle \Phi_b | \alpha_m \rangle = \int_{-\infty}^{+\infty} \Phi_b{}^*\,(x,t)\alpha_m(x)\, dx,$

$$P_b^{ABL} = |\langle \Phi_b | \alpha_m \rangle|^2 = \frac{2\pi}{5\omega\kappa^2}\left(1+\sqrt{1+5\omega^2}\right).$$

(15)

The ABL probabilities Equations (14) and (15) are pseudo-probabilities consistent with Positive Operator-Valued Measure (POVM) formalism [26]. The two channel normalized ABL probabilities, with background channel $P^{ABL}=1$ [28], are:

$$P_f^{NORM}=\frac{P_f^{ABL}}{1+P_f^{ABL}}\equiv\frac{2\pi\left(1+\sqrt{1+\omega^2}\right)}{\omega\kappa^2+2\pi\left(1+\sqrt{1+\omega^2}\right)},$$

(16a)

$$P_b^{NORM}=\frac{P_b^{ABL}}{1+P_b^{ABL}}\equiv\frac{2\pi\left(1+\sqrt{1+5\omega^2}\right)}{5\omega\kappa^2+2\pi\left(1+\sqrt{1+5\omega^2}\right)}.$$

(16b)

Substituting Equations (16a) - (16b) into Equation (9) yields the normalized ABL asymmetry gap.

We compute the joint probability Equation (8), by evaluating the denominator using $\int_{-\infty}^{+\infty}\mathrm{sech}^2(\kappa x)dx=\frac{2}{\kappa}$:

$$\langle\Phi_b|\Phi_f\rangle=\frac{2e^{-2i\omega t}}{\kappa}\sqrt{\frac{16}{5\omega}\left(1+\sqrt{1+5\omega^2}\right)\left(1+\sqrt{1+\omega^2}\right)},$$

(17)

Taking the modulus squared:

$$|\langle\Phi_b|\Phi_f\rangle|^2=\frac{64}{5\kappa^2\omega^2}\left(1+\sqrt{1+5\omega^2}\right)\left(1+\sqrt{1+\omega^2}\right) \quad .$$

(18)

Substituting Equations (13), (15) and (18) into Equation (8):

$$P_{f/b}^{ABL}=\frac{\pi^2}{16\kappa^2},$$

(19)

The two channel normalized is:

$$P_{f/b}^{NORM}=\frac{\pi^2}{16\kappa^2+\pi^2}.$$

(20)

The ω-independence of $P_{f/b}^{ABL}$ renders it blind to T-symmetry breaking records, but κ-dependence measures the total magnitude of the shared forward-backward consistency.

In the strong-coupling limit $\omega \to \infty$, the leading order in the numerators and denominators of forward and backward normalized ABL probabilities grow linearly in ω:$\sqrt{1+\omega^2} \approx \omega$ and $\sqrt{1+5\omega^2} \approx \omega$, then:

$$\lim_{\omega\to\infty} P_f^{NORM} = \frac{2\pi}{\kappa^2}, \quad (21a)$$

$$\lim_{\omega\to\infty} P_b^{NORM} = \frac{2\pi}{\sqrt{5}\kappa^2}. \quad (21b)$$

Equations (21a) and (21b) indicate saturation to finite,κ-dependent constants, showing the amplitude saturation of the underlying soliton ansatz rather than any further ω-dependence. We compute the saturation ratio:

$$\lim_{\omega\to\infty} \frac{P_f^{NORM}}{P_b^{NORM}} = \sqrt{5}, \quad (22)$$

indicating that redistribution is independent of both κ and ω in the saturation regime. Instead it represents the maximum channel imbalance permitted by the underlying quintic-coupling asymmetry. In other words, this shows the maximum split between the forward and backward channels once collapse driving saturates.

2.5. Physical Significance of Diagnostics Convergence in the Strong-Confinement Limit

The norm is a single-time quantity, while the ABL probability correlates two boundary conditions at once, making it a genuine two-time diagnostic [37].In the strong confinement limit $\omega\to\infty$, both the norm ratio and the ABL probability ratio converge to a fixed value $\sqrt{5}$. The fixed value results because strong confinement suppresses the extra information contained in how the two boundary conditions are jointly connected through the stochastic Itō process dynamically established in the quintic-to-cubic ratio of asymmetry [23]. This is a genuine distinguishing time-symmetric ontology from apparent retro-causal artifacts [38].

3.0. RESULTS

3.1.Particle Density and Norm as Complementary Diagnostics of T-Asymmetry

The density maps carry two distinct asymmetry signatures observed on Fig.1. First, at t=0.0 Fig.1(a) the forward (ρ_f) density and backward (ρ_b) densities differ only in overall peaks between them while retaining identical (ω,κ) structure. Fig.1(b), at t=2.0, shows the two density branches having diverged structure: ρ_f flattens into a near uniform plateau across the entire (ω,κ) plane, while ρ_b remains dependent on (ω,κ) throughout. The loss of sensitivity of forward density to (ω,κ) selectively is a signature most directly associated to a directional, collapse-like process rather than reversible redistribution [36], though a two-time quantum-probabilistic effect cannot be established through density profile alone.

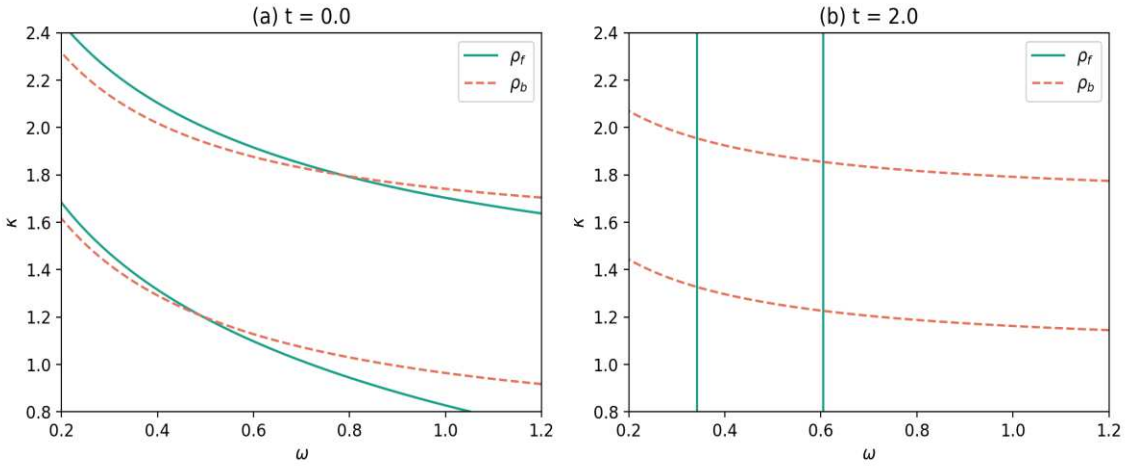


Fig. 1 Contour maps of forward (ρ_f, solid lines) and backward (ρ_b, dashed lines) densities overlaid on the same (ω,κ) axes, at the bookend times t = 0.0 (a) and t = 2.0 (b); contour levels are log-spaced within each branch's own range at that time, so line shape (not absolute level) is the basis for comparison.

The magnitude of the divergence between ρ_f and ρ_b grows continuously with t, Fig.2, with ρ_f amplifying towards saturation while ρ_b is suppressed producing a two-to-three order of magnitude separation by t=2.0. The forward-to-backward ratio grows rapidly from a value $\approx$ 10 in the Low-regime, through $\approx$ 30 at Intermediate, to $\approx$ 1100 at the Strong-regime, showing that the rate of divergence itself grows with driving frequency and wave-number.

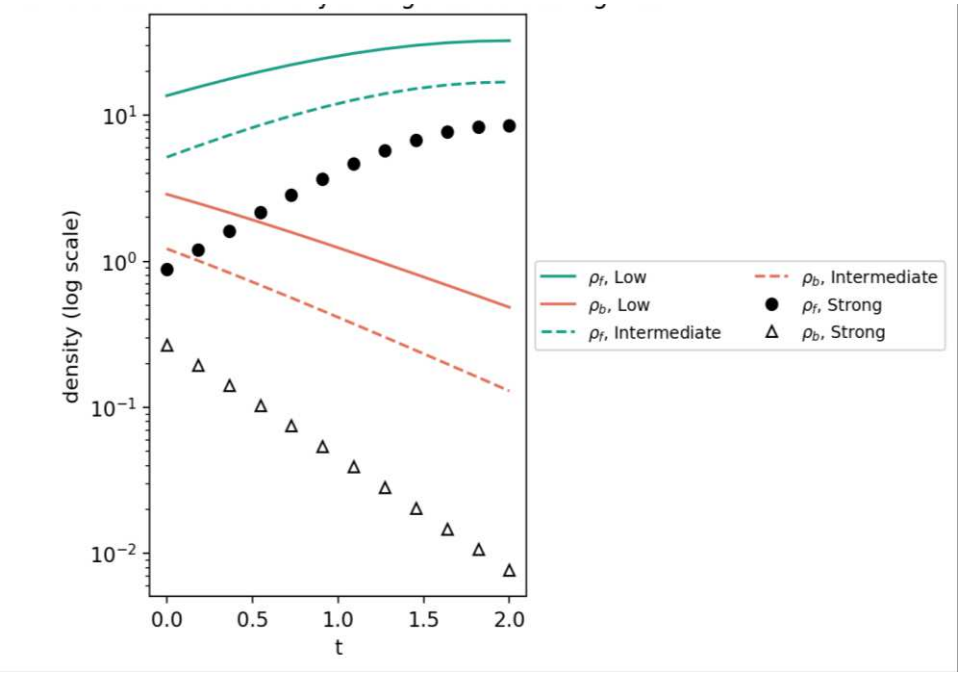


Fig.2. Forward and backward particle density versus t (logarithmic scale) at the Low, Intermediate, and Strong parameter regimes of Table 1 (ω= 0.25, κ= 1.00; ω = 0.50, κ= 1.20; ω = 1.20, κ= 1.80, respectively), overlaid on a single set of axes.

The Norm analysis in Fig.3(a)-(b) further establishes the analytic asymptotic argument (Equ.7). Fig.3(a) indicate rescaling by κ which results in the norm ratio $\frac{N_f}{N_b}$ depending on ω. This necessary precondition provides a qualitative window for κN_f and κN_b collapse onto single curves insensitive of the wave-number κ. Moreover if the dependence on κ still remains as analytically derived in section 2, the strong confinement $\omega \to \infty$ cannot be observed on a single snapshot or well-defined curve. Furthermore, beyond the physically allowed range of ω, Fig.3(b) shows that the norm ratio climbs towards the theoretical saturation $\sqrt{5}$ as ω grows, reaching only near 3.3 to 4.95, but visible still approaching the strong confinement limit as an explicit numerical trajectory, rather than an algebraic assertion. Fig.4 further confirms the norm asymmetry is ω-only, even though both forward and backward norms individually decay with κ at every regime.

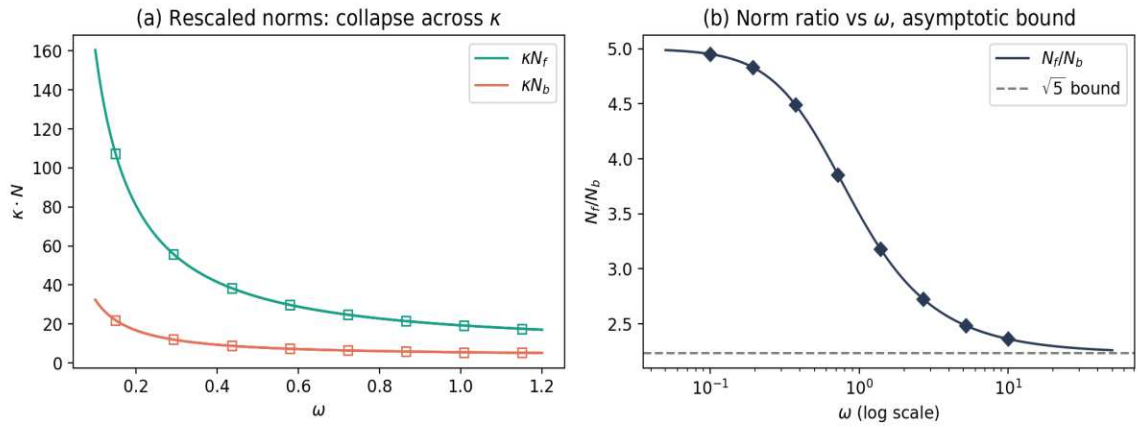


Fig. 3 Collapsed representation of the forward and backward norms and their derived asymmetry, removing redundancy across wave-number regimes. (a) κN_f and κN_b plotted against ω; open markers show the three sampled wave-numbers (κ = 1.0, 1.2, 1.8) landing exactly on a single curve for each branch. (b) N_f/N_b ratio extended over a wider ω range (log scale) with a horizontal reference line at $\sqrt{5} \approx 2.236$, the analytically established asymptotic bound as $\omega \to \infty$

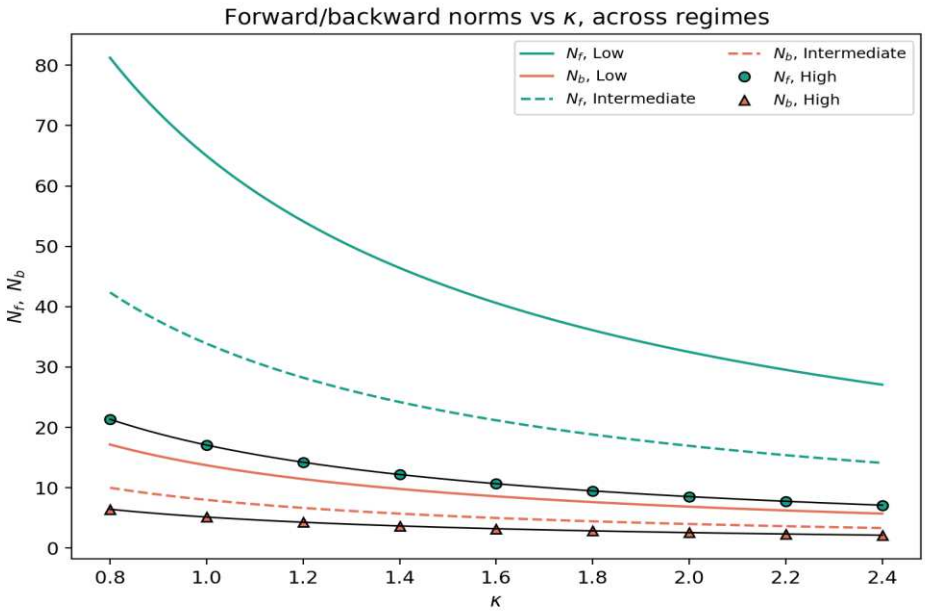


Fig. 4 Forward norm Nf and backward norm Nb as functions of wave-number κ at the Low (ω = 0.25), Intermediate (ω = 0.50), and High (ω = 1.20) trapping-frequency regimes of Table 1, overlaid on a single set of axes. Both norms decay monotonically with κ at every regime, consistent with the 1/κ scaling in Eq. (6a)–(6b); the norm asymmetry ratio N_f/N_b itself is exactly κ-independent, as shown directly in Fig. 3(b).

3.2. A Redistribution Signature from Aharonov-Bergmann-Lebowitz Probabilities

A universal structure is observed across Fig. 5–6: the forward branch P_f^{NORM} lies strictly above P_b^{NORM} at every (ω, κ), with no crossover. The condition $P_f^{NORM} > P_b^{NORM}$ establishing an exact analytical result, indicating how the transition probability split between the forward and backward boundaries, given an intermediate measurement. The forward branch carries the larger ABL weight, but this does not give explicit information on how the system got to the forward branch or evolve afterwards.

Table 1. and Fig. 5(a)-5(c) show the asymmetry gap $|\Delta P^{ABL}|$ grows monotonically with κ at fixed ω, reflecting the stronger κ-suppression of P_b^{NORM} relative to P_f^{NORM}. This arises because the denominator of P_b^{NORM} involves $5\omega\kappa^2$, which is five times larger at the same κ than the $\omega\kappa^2$ term in P_f^{NORM}, depressing the backward branch more steeply. At fixed κ Fig. 5(a)-5(c), $|\Delta P^{ABL}|$ reaches a maximum at an intermediate ω and vanishes as $\omega \to 0$ (both branches → 1).

Table 1.Growth of the asymmetry gap and joint probability across regimes.

Regime	ω	κ	***t***	$\lvert\Delta P^{ABL}\rvert$	Growth	***P(Norm)***
Low	0.25	1.00	0.50	0.0656	Baseline	0.3815
Intermediate	0.50	1.20	1.00	0.1351	+105.87% vs. Low regime	0.2999
Strong	1.20	1.80	2.00	0.2502	+85.13% vs Intermediate Regime	0.1599

The κ-dependent asymmetry growth, Fig. 5(c) does not shrink or grow symmetrically across the κ,ω parameter regimes, as shown by the $|\Delta P^{ABL}|$ values, with (κ, ω) showing +105.87% from low $(\kappa = 1.00, \omega = 0.25)$ to intermediate $(\kappa = 1.20, \omega = 0.50)$ regimes, while +85.13% from intermediate to strong $(\kappa = 1.80, \omega = 1.20)$ regimes.

Unlike the joint probability (κ-only) and the raw redistribution ratio P_f^{NORM}/P_b^{NORM} (ω-only), $|\Delta P^{ABL}|$ varies jointly with both parameters and is not reducible to two independent one-dimensional scans, motivating the full two-dimensional characterization shown here.

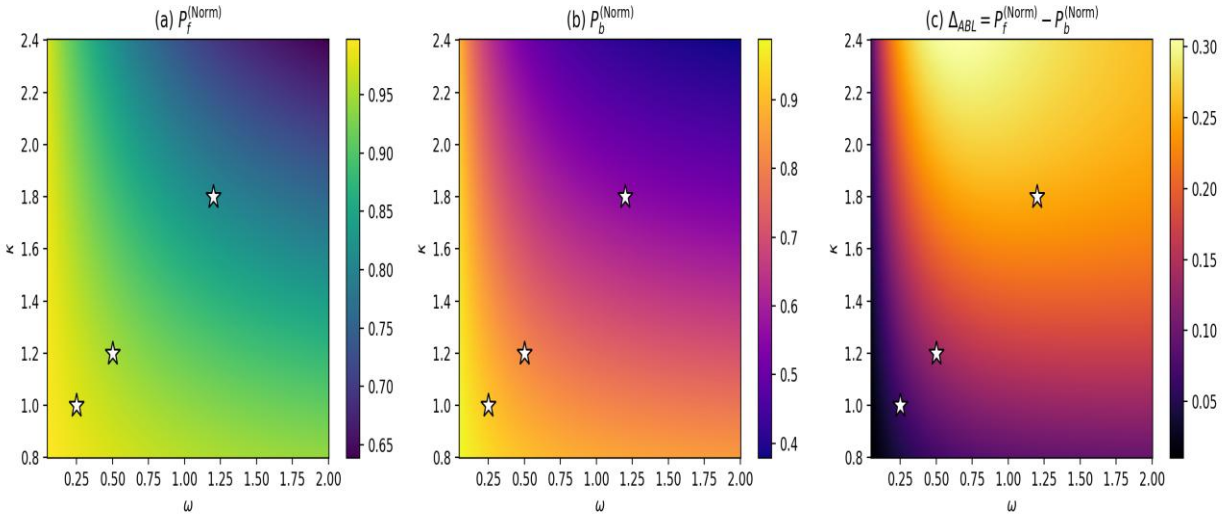


Fig. 5 Two-dimensional heatmaps over the full (ω, κ) plane (ω ∈ [0.05, 2.0], κ ∈ [0.8, 2.4]). (a) P_f^{NORM} ranges over [0.638, 0.997]. (b) P_b^{NORM} ranges over [0.378, 0.987]. (c) The asymmetry gap $|\Delta P^{ABL}|$ ranges over [0.010, 0.305], with no region of the tested domain showing $P_b^{NORM} \geq P_f^{NORM}$. White stars mark the Low, Intermediate, and Strong regimes of Table 1.

The joint probability $P_{f/b}^{NORM}$ (Table 1) is strictly ω-independent, confirming that it probes how much coherence remains as a result of interference between the pre-selected and post-selected boundary conditions when both are directed through the same measurement outcome and is insensitive to the T-symmetry breaking gap encoded by $|\Delta P^{ABL}|$. Its κ-decay (0.491 to 0.097 across κ = 0.8 to 2.4) reflects the falling overlap between the forward and backward histories at higher κ.

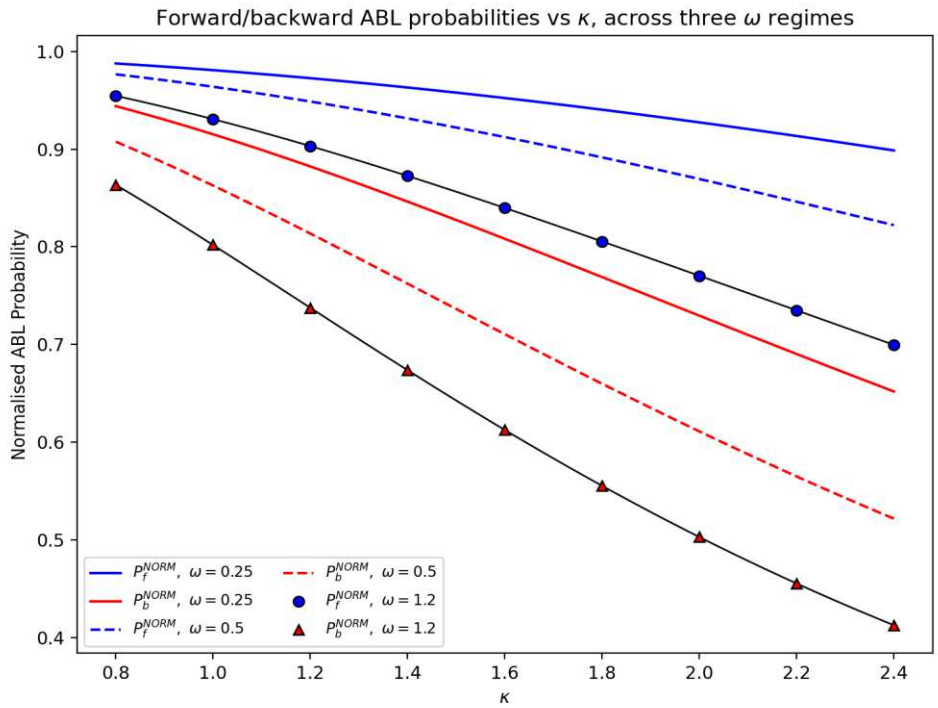


Fig. 6 Forward (P_f^{ABL}, blue) and backward (P_b^{ABL}, red) ABL probabilities versus κ, across three ω regimes overlaid on a single set of axes: solid blue/red lines denote ω = 0.25 and dashed blue/red lines ω = 0.5; for ω = 1.2, a thin black curve traces the continuous trend with blue circles (P_f^{NORM}) and red triangles (P_b^{NORM}) marking nine sampled κ values. P_f^{NORM} lies strictly above P_b^{NORM} at every κ and every ω, with no crossover, confirming the forward branch consistently carries greater ABL weight regardless of driving frequency.

A similar qualitative shape – monotonic suppression of a coherence-type overlap with increasing wavenumber – appears in the collisional decoherence literature, where finer spatial resolution from momentum-transfer resolving power suppresses interference [29, 30]; the correspondence is one of functional form only, since κ here is a fixed structural parameter of the soliton ansatz rather than a rate constant governing a temporal decoherence process. Increasing the collapse driving asymmetry ω does not change how much the forward and backward histories agree with each other overall. What changes is only which of the two acquires more weight in that agreement. This signature indicates that the collapse asymmetry is a redistribution of an already-fixed total between forward and backward channels, not a change in the overall coherence between the histories.

The ω-independence also provides an internal consistency check. Its exact invariance confirms that the stochastic modification in our framework acts as an intrinsic, closed-system redistribution mechanism, already established with the dynamical-collapse construction of Equations (1a) and (1b). This represents a limitation, in that the framework as constructed excludes environmental coupling.

Separately, the disappearance of any dependence on the driving frequency ω from the joint probability agrees with the separation of interference strength and internal phase evolution established for clock interferometers [31], where fringe visibility was shown to depend only on the spatial overlap of wavepackets, not on the internal state of the clock. Englert [32] originally established a duality between visibility and path distinguishability. The joint probability derived here exhibits the same separation: its value is fixed entirely by the spatial (κ-dependent) overlap of the forward and backward envelopes, independent of the driving frequency ω that sets their relative internal phase.

4.0. CONCLUSION

This paper establishes a three T-symmetry breaking diagnostics framework: particle density, norm, and ABL probability, all derived from the same dynamical equations of motion in attractive BEC bright soliton as laboratory. Forward and backward branches of density and norm show that the asymmetry is a real, sigh-definite, single-time phenomenon. In particular, the forward-branch density amplifies toward saturation while simultaneously the backward branch is progressively suppressed, whereas the norm ratio stays bounded across the full (ω,κ) parameter range, sensitive to the driving frequency alone. Together, these signatures indicate a single-time asymmetry, the density and norm do not demonstrate two-time probability structure. The ABL formalism extends asymmetry to a genuine two-time, pre-and post-selected probabilities structure, independent of any specific collapse model. While the individual probability weights, the joint probability, and the asymmetry gap provide qualitative information, the most striking finding is that the collapse driving frequency does not dictate how much the forward and backward histories correlates but only reads which of the two acquires more probability weight in that agreement. This weight redistribution is the time-asymmetry mechanism in the closed soliton system, unlike decoherence-induced T-symmetry breaking in open systems. We propose a controllable BEC bright-soliton

measurement of the ABL probability branches, targeting a null asymmetry gap ($|\Delta P^{ABL}| = 0$), would constitute a direct experimental test of this redistribution mechanism.

ACKNOWLEDGEMENTS

The author gratefully acknowledges Prof. Godfrey E. Akpojotor and Prof.Mike O. Osiele of Delta State University for their roles as supervisors and co-authors on the Time-Asymmetry Energy Modulated Spontaneous Collapse analysis [23] on which the present work builds.

STATEMENTS AND DECLARATIONS

Competing Interests. The author has no relevant financial or non-financial interests to disclose.

Funding. No external funding was received for this work .

Data Availability. No experimental datasets were generated or analysed during the current study. All numerical values reported in Table 1 and Figs.5 and 6 are computed directly from the closed-form analytical expressions given in Equations (9)–(20) and are fully reproducible from those expressions.

REFERENCES

[1] W.H. Zurek, Rev. Mod. Phys. 75, 715 (2003)

[2] M. Schlosshauer, Rev. Mod. Phys. 76, 1267 (2005)

[3] G.C. Ghirardi, A. Rimini, T. Weber, Phys. Rev. D 34, 470 (1986)

[4] G.C. Ghirardi, P. Pearle, A. Rimini, Phys. Rev. A 42, 78 (1990)

[5] A. Bassi, G.C. Ghirardi, Phys. Rep. 379, 257 (2003)

[6] A. Bassi, K. Lochan, S. Satin, T.P. Singh, H. Ulbricht, Rev. Mod. Phys. 85, 471 (2013)

[7] M. Carlesso, S. Donadi, L. Ferialdi, M. Paternostro, H. Ulbricht, A. Bassi, Nat. Phys. 18, 243 (2022)

[8] M. Bilardello, S. Donadi, A. Vinante, A. Bassi, Physica A 462, 764 (2016)

[9] A. Vinante, et al., Phys. Rev. Lett. 119, 110401 (2017)

[10] A. Vinante, et al., Phys. Rev. Lett. 125, 100404 (2020)

[11] M. Carlesso, A. Bassi, P. Falferi, A. Vinante, Phys. Rev. D 94, 124036 (2016)

[12] B. Helou, B.J.J. Slagmolen, D.E. McClelland, Y. Chen, Phys. Rev. D 95, 084054 (2017)

[13] K. Piscicchia, A. Bassi, C. Curceanu, R. Del Grande, S. Donadi, B.C. Hiesmayr, A. Pichler, Entropy 19, 319 (2017)

[14] I.J. Arnquist, et al., Phys. Rev. Lett. 129, 080401 (2022)

[15] S. Donadi, et al., Eur. Phys. J. C 81, 773 (2021)

[16] S.L. Adler, J. Phys. A 40, 2935 (2007)

[17] D. Zheng, Y. Leng, X. Kong, et al., Phys. Rev. Res. 2, 013057 (2020)

[18] A. Tilloy, T.M. Stace, Phys. Rev. Lett. 123, 080402 (2019)

[19] K. Feldmann, R. Tumulka, J. Phys. A 45, 065304 (2012)

[20] E.A. Donley, N.R. Claussen, S.L. Cornish, J.L. Roberts, E.A. Cornell, C.E. Wieman, Nature 412, 295 (2001)

[21] K.E. Strecker, G.B. Partridge, A.G. Truscott, R.G. Hulet, Nature 417, 150 (2002)

[22] B. Øksendal, Stochastic Differential Equations: An Introduction with Applications, 6th edn. (Springer, Berlin, 2003)

[23] I.C. Okoro, M.O. Osiele, G.E. Akpojotor, arXiv:2606.06452 (2026)

[24] D. Anderson, Phys. Rev. A 27, 3135 (1983)

[25] M. Waegell, E. Cohen, A. Elitzur, J. Tollaksen, Y. Aharonov, Proc. Natl. Acad. Sci. U.S.A. 120, e2018437120 (2023)

[26] M.A. Nielsen, I.L. Chuang, Quantum Computation and Quantum Information (Cambridge University Press, Cambridge, 2010)

[27] M.H. Anderson, J.R. Ensher, M.R. Matthews, C.E. Wieman, E.A. Cornell, Science 269, 198 (1995)

[28] Y. Aharonov, P.G. Bergmann, J.L. Lebowitz, Phys. Rev. 134, B1410 (1964)

[29] K. Hornberger, J.E. Sipe, Phys. Rev. A 68, 012105 (2003)

[30] L. Badurina, C. Murgui, R. Plestid, Phys. Rev. A 110, 033311 (2024)

[31] Z. Zhou, Y. Margalit, D. Rohrlich, Y. Japha, R. Folman, Class. Quantum Grav. 35, 185003 (2018)

[32] B.-G. Englert, Phys. Rev. Lett. 77, 2154 (1996)

[33] M. Ridley, Quantum Rep. 5, 496 (2023)

[34] M. Ridley, E. Adlam, Quantum Stud. Math. Found. 12, 9 (2025)

[35] V.V. Konotop, J. Yang, D.A. Zezyulin, Rev. Mod. Phys. 88, 035002 (2016)

[36] A. Smirne, A. Bassi, Sci. Rep. 5, 12518 (2015)

[37] S. Jin, arXiv:2204.12328 (2022)

[38] M.S. Leifer, M.F. Pusey, Proc. R. Soc. A 473, 20160607 (2017)